Sensors & Actuators: B. Chemical 321 (2020) 128590

Contents lists available at ScienceDirect

Sensors and Actuators B: Chemical

journal homepage: www.elsevier.com/locate/snb

Fabrication method of multi-depth circular microchannels for investigating arterial thrombosis-on-a-chip

Thanh Qua Nguyen[a,c], Woo-Tae Park[a,b,*]

[a] Convergence Institute of Biomedical Engineering and Biomaterials, Seoul National University of Science and Technology, Republic of Korea
[b] Department of Mechanical and Automotive Engineering, Seoul National University of Science and Technology, Republic of Korea
[c] Center for Bionics, Korea Institute of Science and Technology, Republic of Korea

ARTICLE INFO

Keywords:
Partially cured PDMS
Circular channel
Thrombosis-on-a-chip
Concentric and eccentric stenosis

ABSTRACT

The circular cross-section of the microchannel plays an important role in recapitulating the physiological relevance of an in-vitro model of blood vessels. In this study, we demonstrate a simple process for turning the single depth of a rectangular microchannel of the mold into a multi-depth circular polydimethylsiloxane (PDMS) microchannel of the replica. The method uses inflated air pressure to deform a partially cured PDMS with simple bench-top equipment. We can produce a wide range of circular microchannels with diameters from 100 μm to 500 μm. Based on the self-aligning and bonding principles of partially cured PDMS, this technique can eliminate oxygen plasma bonding and tedious alignment processes. The bonding strength based on the partially cured PDMS can obtain 375 kPa, which is comparable with oxygen plasma bonding. The fabrication parameters, such as the partial curing time of PDMS and the applied pressure, are controlled well to obtain various channel geometries from elliptical to circular cross-sections. We applied the fabrication scheme to reconstruct the geometry of the thrombosis blood vessel in a microfluidic device. Four different geometries of stenosis vessels were successfully produced for investigating the influence of the occlusion shape on thrombus formation. The platelet deposition along the post-stenosis channels was quantitatively observed under time-lapse fluorescence microscopy. Our results indicate that the accumulation of platelets for downstream stenosis is slower and more stable for a concentric stenosis lesion than for an eccentric stenosis lesion. This thrombosis device can be used in real-time clotting analysis models and for antithrombotic drug testing.

1. Introduction

Arterial thrombosis is the formation of a blood clot within an artery and it is a complex process that comprises multiple steps. The mechanism of thrombosis involves various factors based on the blood components. This includes the von Willebrand factor (vWF), the geometry of the vessel, the shear rate, the prothrombogenic surface (collagen), and the platelet function. An essential early event in the thrombus initiation under high pathologic flow (shear rate $> 5000\ s^{-1}$) is the interaction between vWF and the platelet's receptor GPIbα [1,2]. A pathological shear rate happens at the stenosis of the blood vessel, namely atherosclerosis. Rupture of the atherosclerotic plaque can result in vascular diseases such as acute coronary syndromes and ischemic stroke [3]. Therefore, a better understanding of the mechanism of thrombus formation in atherosclerotic vessel segments is essential to improving current antithrombotic medications.

Conventional models used to study thrombosis include in vivo animal models, which ranges from small animals (e.g. zebra fish, mice, etc.) to larger animals (e.g. dogs, pigs, nonhuman primates, etc.) [4], and in vitro models in the form of parallel-plate flow chambers and rotating cone plate viscometers [5,6]. The small animal models allow for investigating the role of genetic variation and different clotting factors in thrombus formation. However, the genetic and physiological differences in comparison to human models limits them to recapitulate human disease conditions. Large animal models offer increased physiological relevance to humans, but these experiments are not efficiently conducted in academic laboratories and have ethical restrictions [7]. Therefore, in vitro models can be considered as the first choice to model thrombotic diseases. With parallel-plate flow chambers, the flow rates can be easily controlled by using syringe pumps that can induce various wall shear stress over the surface-coated extracellular matrix (e.g. collagen, fibronectin) and thrombosis factors (e.g. vWF or tissue

* Corresponding author at: Convergence Institute of Biomedical Engineering and Biomaterials, Seoul National University of Science and Technology, Republic of Korea.
E-mail address: wtpark@seoultech.ac.kr (W.-T. Park).

https://doi.org/10.1016/j.snb.2020.128590
Received 1 March 2020; Received in revised form 6 July 2020; Accepted 11 July 2020
Available online 18 July 2020
0925-4005/

factor) [6]. Although many researchers use this system to investigate the effect of the shear stress on the platelet function and coagulation factors, the accurate anatomy of a blood vessel is not replicated in these chambers. The other commonly used platelet function test is the cone-and-plate viscometer. It involves the rotating cone to create the shear stress on the stationary plate surface [8]. These devices require a large amount of blood volume and low-throughput. More importantly, these devices cannot mimic the completed functions of the three-dimensional (3D) geometry of the vascular system and the natural physiology of blood flow. These limitations have been countered by the recent development of microfluidic devices that can be engineered to offer a better physiological representation of human vascular thrombosis.

In recent decades, microfluidics have played an essential role in the field of biomedical engineering due to its high throughput, automation capabilities, and their low-cost fabrication [5,9]. Microfluidic devices are a powerful tool to recapitulate the pathophysiology of the blood flow with various wall shear rates in the channels [10–14]. The major advantages of microfluidic devices are its low blood sample requirements, short analysis time, precise control of dimensions, and high repeatability over a large number of experiments [7]. To mimic the arterial physiology in a microfluidic device, the high shear rate and shear gradient play critical roles in the activation of the vWF along with platelet adhesion and aggregation [7,8]. Further, platelet adhesion, activation, and thrombus growth depend significantly on the microchannel geometry. However, there are several geometric constraints within current standard microfluidics manufacturing. This includes the rectangular profile and the limit of the channel depth to allow thrombus growth [17]. Owing to the limitation of the two-dimensional (2D) based microfabrication techniques of microfluidic devices, the channels used to study pathological flows often have a rectangular cross-section with a high surface-to-volume ratio [18,19]. The single depth based microfluidics channel has narrowed the channel width while the microchannel depth stayed constant [5,7,8]. Thus, very high shear rates are hard to achieve with conventional manufacturing methods [17,19]. Consequently, only 3D circular microchannels are truly representative of human vessel geometries.

Therefore, it is of great interest to researchers to fabricate the circular channels that mimic the complex flow conditions of cardiovascular disease at various stages. The circular geometry of a microchannel provides the uniform shear stress along with the walls of the channels [20,21]. Several strategies have been employed to produce a microfluidic channel with a circular cross-section. The typical approach is to fabricate the semi-circular channels in two halves that, after being transferred to PDMS, are aligned and bonded to form the circular channel. This approach can be observed with a reflowed positive photoresist [22], laser engraving or micro-milling [23], grayscale dual projection lithography [24], isotropically etched silicon wafers [25], a PDMS membrane deformation technique [26], and extrusion printing of mold using a thixotropic ink [27]. Such techniques can produce uniform semi-circular channels; however, the creation of circular channels requires tedious alignment and bonding. Misalignment during plasma bonding is a particularly major issue when fabricating branched or multiple blood vessel channels. The second approach is using a PDMS prepolymer to modify the rectangular channels to become a circular channel by coating the liquid PDMS on the channel surface [28]. While this technique provides a low-cost way to build single depth circular channels, it is challenging to achieve repeatability and channel size control.

Another approach is directly fabricating the circular channel or sacrificial template using 3D printing or inserting circular metal wire [29–32]. It can be used to fabricate a 3D structure directly or to produce a 3D sacrificial template for soft lithography. Recently, Andries van der Meer et al. presented a study that mimicked 3D vascular structures of arterial atherosclerosis. They combined the data of computed tomography angiography and 3D stereolithography printing to construct the vessel templates. The PDMS microchannel was generated with PDMS casting and by manually breaking the 3D printed template [11]. Therefore, this approach can prototype single and straight stenosis microchannels. However, the current 3D printing technique for microfluidic applications still has its limitations. This includes a relatively larger lateral resolution ($> 25\,\mu m$) [11] and the issue of high surface roughness that can negatively influence microfluidic flow and the optical clarity.

Overall, the presented method to fabricate the multi-depth circular microchannels that can replicate vascular geometry is complex and costly. Recently, our group introduced a novel method that uses partially cured PDMS that is combined with thermal air expansion molding to fabricate a semi-circular or circular microchannel with low-cost and straightforward benchtop equipment [33,34]. The deformation depth of the circular channel is dependent on the partially cured time of the PDMS and the curing temperature. This method demonstrates the ability to create PDMS circular channels with diameters ranging from 25 μm to 150 μm with a smooth inner channel surface. However, it is difficult to obtain channels larger than 200 μm because the deformation pressure inside the closed channel increases due to the thermal effect. This is not enough to push down the partially cured PDMS during the fabrication. In this study, we developed a method to fabricate circular channels that range in diameter from 100 μm to 500 μm by precisely controlling the gas pressure inside the fabricated channels. We investigated the effect of the fabrication parameters such as the partial curing time and applied a pressure to obtain the desired circular microfluidic channel. Finally, as a proof-of-concept, multiple stenosis channels were fabricated to recapitulate the 3D geometry of the stenosis blood vessels. The flow simulations verified that the circular geometry can create the appropriate wall shear rates that are found during in vivo thrombosis [13,16]. The thrombosis formation during perfusion of whole blood for the concentric and eccentric morphological vessel was also characterized.

This article is organized as follows. 1) Optimize the fabrication conditions for making the desired circular microchannels from 100 μm to 500 μm. 2) Using an optimal parameter to fabricate multiple 3D stenosis channels that mimics the different stenosis geometries. These include concentric and eccentric at 63 % and 84 % stenosis, respectively. 3) Time-lapse of the thrombosis formation and stability of the thrombus by perfusing the human whole blood through the collagen-coated circular channels under the pathological flow conditions of eccentric and concentric stenosis. This manuscript describes the materials and methods for the experiments. In addition, this manuscript presents the results and the discussion from the experiments followed by the conclusion.

2. Material and methods

2.1. Material and equipment

Sylgard 184 silicone elastomer (PDMS) was purchased from Dow Corning, and SU-8 negative photoresist was purchased from Microchem. The PDMS that was used for this work was a mixture of a base precursor and a curing agent with a ratio of 10:1 (w/w). The PDMS mold with a ratio of 10:1 (w/w) was replicated from the SU-8 master mold using soft lithography that was cured in an oven at 90 °C for 1 h. We prepared 3% of the hydrophilic polymer hydroxypropyl-methylcellulose (HPMC) solution to follow the procedure [35]. To create the surface treatment PDMS, the PDMS stamp was submerged inside the HPMC solution for 30 min at 70 °C. Then, it was washed three times with diluted water and dried in an oven for 15 min. A syringe pump (NE-4000 New Era Pump, UAS) was used to manipulate the air pressure in the microchannel. High resolution of the differential pressure sensor (Phidgets-1126, Phidget Inc) was used to measure the pressure in the microchannel. The detected pressure range was from -25 kPa to $+25$ kPa. The Arduino Orange board was used for reading out the pressure sensor signal and it was connected to the computer through

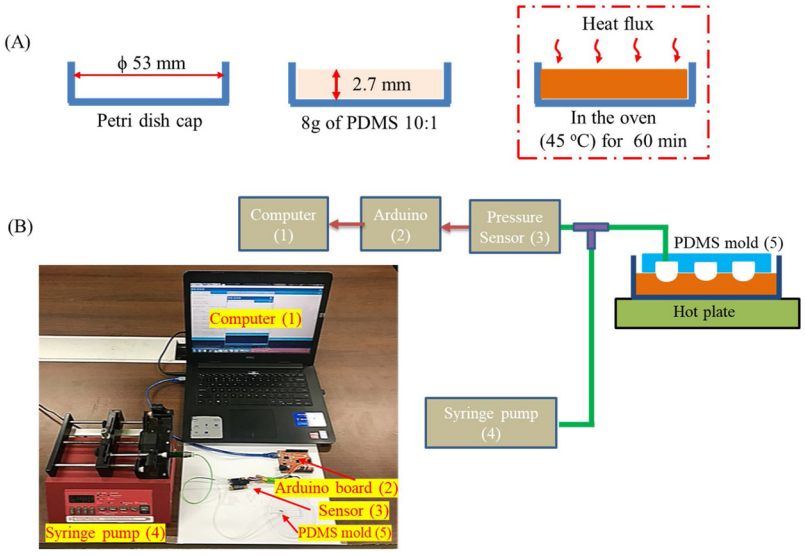

Fig. 1. Partially cured PDMS procedure and experimental setup. (A) The procedure of partially cured PDMS. (B) The experiment setup of the fabrication with computer, Arduino board, pressure sensor, syringe pump, and PDMS mold.

the Arduino interface. Teflon tubes (0.8 mm in inner diameter) were used to connect the syringe with a pressure sensor and the PDMS mold. The 3 mL syringe (Norm-Jet, Germany) was filled with diluted water to prevent air leakage during pumping. The flow rate of the pump was set to 5 μL/min to create the uniform deformation of the partially cured PDMS surface.

2.2. Preparation of partially cured PDMS and fabrication process

Partially cured PDMS was prepared following the procedure in Fig. 1A. The PDMS was made by mixing the base and curing agent at a ratio of 10:1 (w/w), then it was degassed to remove the trapped air bubble. Then, we poured 8 g of PDMS pre-polymer on the 53 mm inner diameter of the Petri dish cap and it was partially cured at 45 °C in the convection oven. After 60 min, 65 min, and 70 min of curing in the oven, the PDMS was in a gelatinous stage with a sticky surface [36]. Fig. 1B shows the experimental setup with the syringe pump, hot plate, pressure sensor, and computer. The syringe pump was set with the flow rate at 5 μL/min. The signal of the inflated pressure was monitored by a pressure sensor, read out by the Arduino board, and it was visualized on a computer.

The procedure used to fabricate the circular microchannels is described in Fig. 2. The PDMS mold was replicated from the SU-8 master by soft-lithography and then it was treated with HPMC solution to modify the contacting surface [35]. The surface treatment prevents the tearing of the PDMS mold. The PDMS mold was carefully contacted with the partially cured PDMS surface that was prepared with the procedure shown in Fig. 1A. Then, the air pressure in the channel was gradually increased after setting the air inflation of the syringe pump. Due to the inflated pressure, the partially cured PDMS surface was pushed down to form the semi-circular channel. The deformation of the partially cured PDMS can reach a quiescent state after stopping the air inflation. The balance between the PDMS stiffness and the channel's inner pressure finally defines the channel profile. Then, the stack was treated on a hot plate at 95 °C for 20 min to fully cure the PDMS. The internal pressure inside the microchannel was continuously monitored. The semi-circular microchannel stamp was peeled off from the mold after being fully cured on the hot plate. To obtain the circular channel, we repeated the process in Fig. 2B to D with the semi-circular PDMS stamp as a mold. However, the PDMS mold in the following process was not treated with the HPMC solution to form a good bonding strength between the two halves of the PDMS. The bonding between the partially cured PDMS with different surface treatments is characterized and discussed in section 3.2.

2.3. Master mold design and fabrication

To characterize the channel cross-section under the different fabrication parameters, we designed the serial microchannel with widths of 500, 400, 300, 200, and 100 μm (Fig. 3A). The master mold was fabricated based on the standard photolithography with a SU-8 negative photoresist. The final mold thickness was 140 μm.

2.4. Characterization of the fabricated channels

The depth of the fabricated channel was characterized by obtaining a cross-section using a razor blade knife, and the dimensions were measured under an optical microscope (BX51, Olympus Japan) and the accompanying software (JNOPTIC capture 2.2, Korea). Scanning electron microscopy (SEM) (Tescan Vega3, Czech Republic) was used to obtain the 3D geometry of the PDMS microchannel.

2.5. Whole blood staining and perfusion

Blood samples were collected from three healthy, drug-free adult volunteers with their written consent. Blood was drawn through a 21-gauge needle into syringes that were prefilled with 3 U mL^{-1} of heparin (Sigma) as an anticoagulant. The experiments were initiated within 30 min after drawing the blood.

To initially activate the platelet adhesion on the PDMS surface, the PDMS channels were treated with 100 μg ml^{-1} fibrillary collagen type I (Sigma Aldrich) overnight at 4 °C. Then, the channels were washed with 1% bovine serum albumin solution followed by 1X phosphate-buffered saline before blood perfusion [13].

Before performing perfusion of the whole blood sample into the device, the platelets in the whole blood samples were stained with 2 μg ml^{-1} of 3,3′-dihexyloxacarbocyanine iodide ($DiOC_6$, Sigma Aldrich) and they were incubated at 37 °C for 10 min. The 2 mm inner diameter of the flexible silicone tube was used to connect the syringe to the chip and the chip to the waste reservoir. The blood was perfused through the microfluidic device using the Harvard PHD-2000 syringe pump (Harvard Apparatus, USA) at a flow rate of 3 mL/hr. Platelet aggregation was monitored by using a Nikon Ti Eclipse fluorescent microscope (Nikon, Japan) with an excitation and emission wavelength of 485 nm

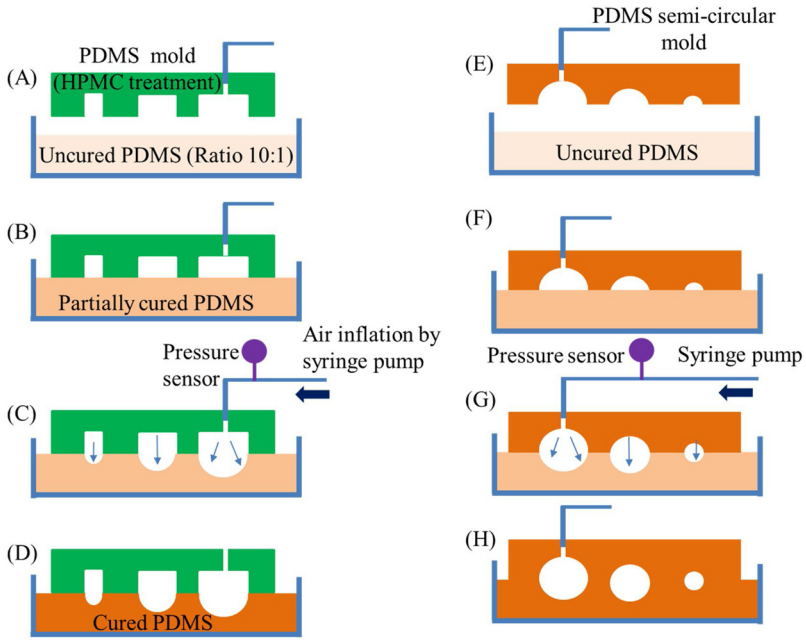

Fig. 2. Schematic of fabrication process of semi- and circular microchannel. (A) The PDMS mold after HPMC treatment and the partially cured PDMS. (B) The mold and partially cured PDMS brought into contact. (C) Air inflated into the channel by using the syringe pump. The partially cured surface was deformed by applied pressure. (D) Partially PDMS stack was fully cured on the hot plate. (E-H) Repeated the fabrication process to get the full-circular channel by using the semi-circular as a mold.

and 520 nm, respectively. Image acquisition was controlled through Metamorph 6.0 (multi-dimension acquisition). The stack images were acquired at one frame per second, which were captured for 5 min during the perfusion. ImageJ software was used to post-process the captured images. The region of interest (ROI) was defined as 1000 μm in length and the stenosis boundary. The fluorescence intensity of the platelets was analyzed in the area along the stenosis channel with a 500 μm length at the post-stenosis channel.

2.6. Thrombosis-on-a-chip

To investigate the effect of the stenotic geometries on the platelet aggregation, we designed and fabricated four parallel channels with separated inlets and a common outlet. There are two types of stenosis channels, namely concentric and eccentric. The width of the non-stenosis channel, 63 % stenosis, and 84 % stenosis were 500 μm, 200 μm, and 100 μm, respectively. This design was intended to be the proof of concept by applying the clinically derived physiological range (< 2000

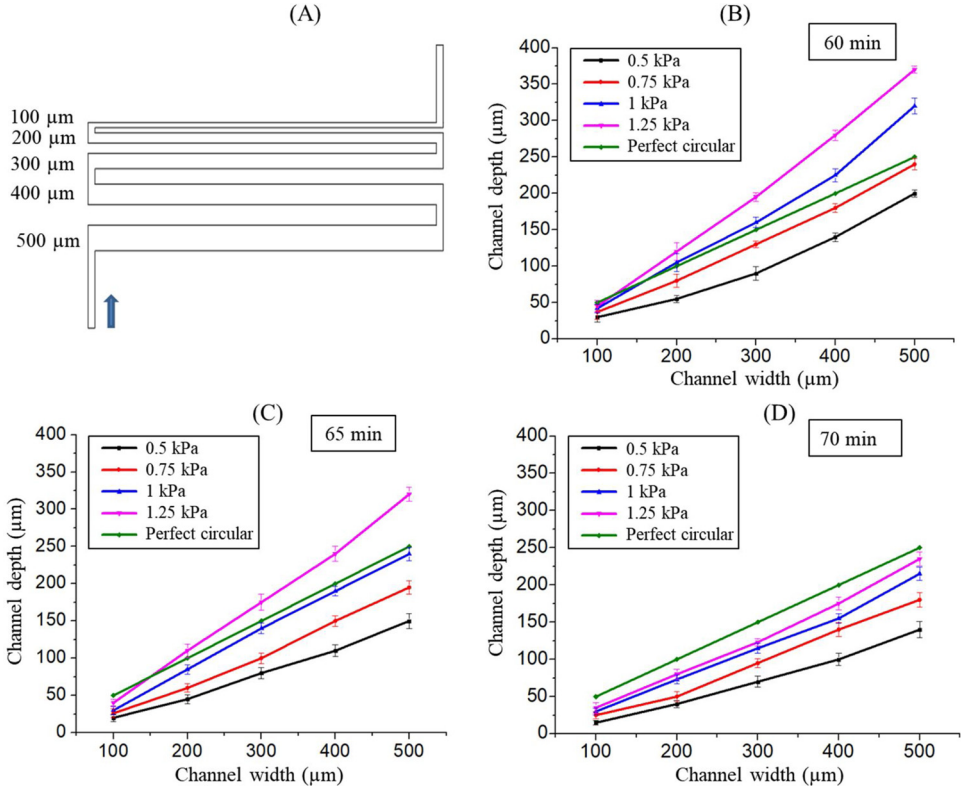

Fig. 3. Characterization the depth of channel. (A) The serial channels use to characterize the channel deformation with the width of 100 μm, 200 μm, 300 μm, 400 μm, and 500 μm. The arrow shows the direction of inflated air. (B), (C), (D) the deformation of channel at partial curing of 60 min, 65 min, and 70 min.

s^{-1}) for 63 % stenosis and the pathological flow of 84 % stenosis ($> 10{,}000\ s^{-1}$) [9,37]. We compared the thrombosis formation at the same stenosis percentage channel with different concentric and eccentric geometries. The slopes of the stenosis, the wall shear rate profile, and the maximal flow elongation rates are all similar to the atherosclerosis found in the arterial vessel [10,11]. After fabrication, the channels had an elliptical geometry with the major axis *a* and minor axis *b*. The average depth of the non-stenosis, 63 % stenosis, and 84 % stenosis channels were 400 μm, 150 μm, and 65 μm, respectively. Based on the major and minor axes of the elliptical cross-section, we calculated the hydraulic diameter of the non-stenosis and stenosis channels. Then, the stenosis percentage was calculated with the following equation, where D_i and D_0 are the hydraulic diameters of the stenosis and the normal geometry, respectively.

$$\%\ stenosis = \frac{D_o - D_i}{D_o} \times 100\%$$

The stenosis of the blood vessels was designed by gradually reducing the channel width from a healthy vessel diameter of 500 μm to the stenosis vessel diameter of 100 μm and 200 μm. The stenosis length was 1000 μm. The angles of reduction and expansion were symmetrical. Platelet aggregation in the stenosis outlet region was the most prominent at 60–80 % lumen reduction for the pathological flow conditions [10]. The thrombosis device was fabricated for conditions with a 65 min partially cured time, a 45 °C partially cured temperature, and a 1 kPa inflated pressure to generate the semi-circular and circular multi-depth channels that mimic the concentric and eccentric stenosis of the blood vessel. The depths of the fabricated channels are 400 ± 15 μm, 150 ± 12 μm, and 65 ± 8 μm (n = 3) for the normal channel, the 63 % stenosis channel, and the 84 % stenosis channel, respectively. The channel structures are different from the channels that were used to characterize the fabrication method; therefore, after fabrication, we cut the device to measure the dimensions of the stenosis channel. The two ends of the stenosis area are 500 μm wide; hence, the deformation for the 100 μm and 200 μm wide stenosis is different from the optimal dimensions that are shown in the fabrication. The errors in the channel geometry affect the wall shear rate and the percentage of the stenosis. Therefore, it can result in different thrombosis formation. The errors of the channel geometry or the threshold of the stenosis percentage will be investigated in future studies.

3. Results and discussion

3.1. Characterization of channel geometry

Three important parameters directly affected the profile of the fabricated channel: 1) the width of the mold, 2) the stiffness of the partially cured PDMS, and 3) the applied pressure. Fig. 3A shows the design of a master mold with five different widths, including 100, 200, 300, 400, and 500 μm. Owing to the standard photolithography-based microfabrication, the SU-8 master mold had the rectangular cross-section with a planar microchannel that was 140 μm in height (data not shown). The stiffness of the partially cured PDMS was controlled by varying the partial curing time while the curing temperature and the amount of PDMS was fixed. The higher the curing temperature, the shorter the gelation duration we obtained [36]. However, a shorter gelation duration can cause errors during fabrication. Thus, to precisely control the stiffness of the partially cured PDMS and to reduce the effect of the heat gradient, we cured the PDMS in a convection oven at 45 °C; this slowed down the gelation process and extended the gelation duration. With 8 g of PDMS and a 45 °C curing temperature, the partial curing time (or the gelation duration) ranged approximately from 60 min to 70 min. The PDMS under the gelation stage was suitable for the fabrication of the circular channel by inflated air. The cure time for the partially cured PDMS was selected as 60 min, 65 min, and 70 min. The applied pressure was manipulated by a syringe pump and it was monitored by the pressure sensor. Four different pressures (P = 0.5 kPa, 0.75 kPa, 1 kPa, and 1.25 kPa) were used to generate the circular channels. The standard deviation of the applied pressure was ± 0.05 kPa. The relatively small pressures ensured that there was a good seal between the mold and the partially cured surface. During the experiment, there were no signs that unsealing occurred between the mold and the partially cured surface. Since the serial channels are connected to each other, the pressure inside the channel is the same in comparison to the partially cured PDMS deformation. The bigger width deformed more than the smaller width. We assumed that the partially cured PDMS was a flexible membrane; therefore, the deformation in each channel depended on the channel width and the applied pressure [26]. To evaluate the depth of the fabricated channel, we defined the perfect circular channel where the depth was half of the designed channel width. As the deformation depth approached the perfect circular channel, the channel width approached a nearly perfect circular value. Fig. 3B shows that for the 60 min partially cured condition, the deformation depth of the channel is lower than the perfect circular channel at 0.5 kPa and 0.75 kPa, and it is higher than the perfect circular channel at 1 kPa and 1.25 kPa.

At 65 min for the partially cured condition, the 1 kPa pressure shows that the depth is nearest to the perfect circular channel, while the 0.5 kPa and 0.75 kPa depths are lower than the perfect circular channel. At 1 kPa and 65 min for the partially cured condition, the channel deformation was 240 ± 9 μm, 190 ± 6.5 μm, 140 ± 7 μm, 85 ± 6.5 μm, and 30 ± 6 μm for the channel widths of 500 μm, 400 μm, 300 μm, 200 μm, and 100 μm, respectively. These conditions were determined to be the optimal conditions for making the channel with a nearly circular construction that mimicked the blood vessels. For the 70 min partially cured condition, the whole channel depths were lower than the perfect circular channel due to the high surface stiffness of the partially cured PDMS. The increase in the applied pressure did not significantly affect the channel depth.

A change in the cross-section geometry from elliptical to over-circular can be obtained with an inflated pressure during the fabrication of the first and second halves of the channel. Fig. 4A shows the cross-section of the semi-circular fabricated channel from 200 μm to 500 μm for the applied pressures of 0.5 kPa, 1 kPa, and 1.25 kPa at a partial curing time of 65 min. We defined the deformation depth of the channel as (1) much lower than half of the mold width, (2) close to half of the mold width, and (3) greater than half of the mold width. When we combined the conditions of (1), (2), and (3) to make the full channel, we were able to generate six channel geometries as shown in Fig. 4B. The full channel geometry depends on the semi-circular width and the combination of the fabrication parameters. The results of the full channel from 100 μm to 500 μm of the channel width are shown in Fig. 4C. The condition (1 − 1) shows the lowest channel depth with an elliptical profile at all channel depths, in which condition (3 − 3) generates the biggest channel depth. In addition, at 300 μm, 400 μm, and 500 μm for condition (3 − 3), the channel depth is over the perfect circular depth. The condition (2 − 2) and (2–3) generates the closest shape to a perfect circular channel. Here we define almost perfect circular channel. The almost perfect circular channel is defined as the condition when the full channel height measurement equals the full channel width measurement. Even if the height and width is the same, this does not guarantee a perfect circle because the top and bottom parts are not symmetric.

We fabricated the microchannel with five different widths from 100 μm to 500 μm. Since the five channels are connected and are under the same fabrication pressure, the deformation depth of the different channel width differs with a higher deformation ratio (deformation depth/ channel width) on a bigger channel. Therefore, the almost perfect circular channel for all five channels may not be obtained at the same time. Instead, we can select the appropriate condition for the pressure and partial curing time to make an almost perfect circular channel for the single width channel. Thus, the almost perfect channels

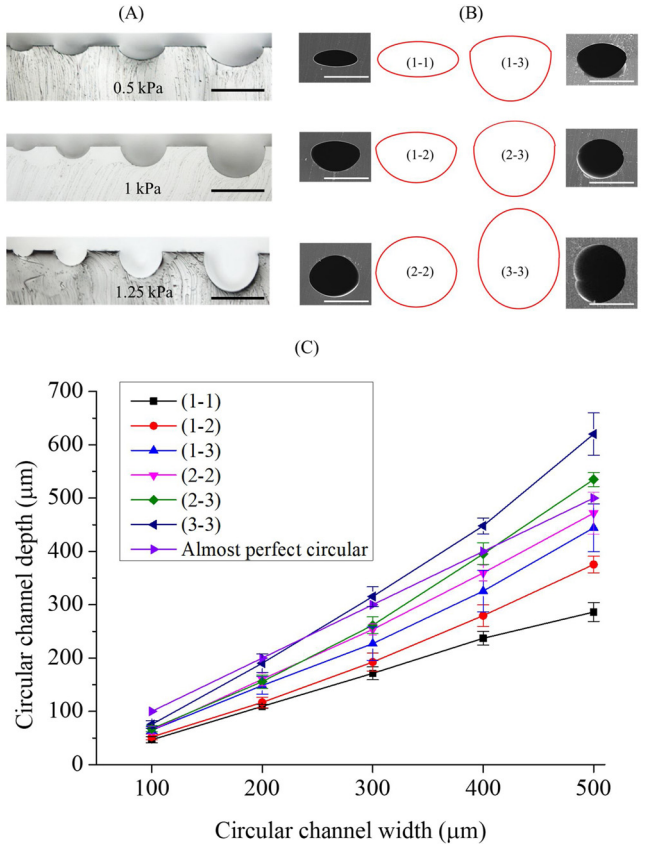

Fig. 4. Bright field images of the semi-circular channels from 200 μm to 500 μm at different fabrication pressure of 0.5 kPa, 1 kPa, and 1.25 kPa. (B) SEM image of the channel cross-section with different fabrication conditions. We define (1) is the condition for under deformation, (2) is the semi-circular, and (3) is the over deformation. Various cross-sectional channels of 500 μm in width can be obtained by combining the different fabrication conditions of first half and second half of the channel. Scale bar, 500 μm. (C) The relationship between formed circular channel shape and semi-circular channel shape of different channel width.

are achieved at channel width of 200 μm and 300 μm in case (3 – 3), 400 μm in case (2–3), and 500 μm in case (2 – 2). The channel width of 100 μm cannot obtain the almost perfect circular channel for the six combinations. This issue can be a limitation of this method when fabricating the multi-depth channel. However, in this study, we had the advantage of being able to generate various types of microchannels using the same master mold, thereby reducing the fabrication cost and time.

3.2. Evaluation of bonding strength of the device

To evaluate the bonding strength of the PDMS device that was made by the partially cured PDMS, we designed the testing setup with a pressure regulator, as shown in Fig. 5A [38]. The mold chamber was fabricated by performing standard photolithography with a negative SU-8. Then, we used soft lithography of the PDMS (10:1) to replicate the top layer of the testing chamber. The testing chamber was 0.1 mm in height and 5 mm in diameter, as shown in Fig. 5B. The dimensions of the top PDMS are 100 mm x 100 mm x 3 mm (width × length x height). A sharp 23 G needle was used to punch a hole on top of the PDMS for the tubing. We used a 10 mm 21 G blunted stainless tube to connect the air tube to the top of the PDMS. Owing to the huge difference in the diameters of the stainless tube (outer diameter of 0.819 mm) and the PDMS hole (0.337 mm), the tubing can be secured under a pressure of 500 kPa. The bottom of the PDMS layer was partially cured in an oven at 45 °C for 65 min.. In the case of partial curing of the PDMS bond, there are two conditions of the top PDMS: one is treated with a HPMC solution, and the other one is non-treated. The two partial bonds were compared to oxygen plasma bonding. For oxygen plasma bonding, the top and bottom of the PDMS were bonded after exposure in the plasma chamber (at 100 W, 600 mTorr, and 90 s). For burst pressure testing, the regulated air pressure from the compressed air line was supplied to the testing chamber through the pressure regulator. The air pressure slowly increased to 25 kPa at time intervals of 10 s until the bonding failed. The bursting surfaces for each bonding condition are shown in Fig. 5C. This reveals the difference on the surface texture after the bonding failed. Failure of the bonds occurred via a concentric delamination at the top and the bottom of the PDMS (Fig. 5C, red arrows). The bonding failure area is indicated by the yellow arrow in Fig. 5C. The surface texture is different between the plasma bonding and the partial bonding. We observed the tearing out on the plasma bonding surface after the bonding was broken. By contrast, with partial bonding, delamination of the top and bottom PDMS layer occurred with a clear surface for the bonding failure area. The surface of the partially cured PDMS works as an adhesive layer. Therefore, the partially cured surface can produce the perfect confluent with the solid surface while bonding. It allows partial bonding to withstand the delamination pressure. With plasma bonding, the two solid PDMS surfaces are brought into contact after plasma activation to form covalent bonding. Solid and solid contacting can cause less confluence between the two surfaces. Although PDMS plasma bonding forms a covalent bond, the less confluent surface can reduce the bonding strength. The comparison of the two partially cured PDMS bonds and the plasma bonding is shown in Fig. 5D. The average burst pressure of the partially bonded PDMS treated with HPMC was 150 kPa. The low bonding strength can be attributed to the straight-forward detachment of the mold after the first semi-circular section was fabricated. The bonding strength of the oxygen plasma matched well with a previous study for the average bonding strength of 300 kPa [38]. Among the three bonding conditions, the partially cured PDMS bonding strength was the highest at 375 kPa. This bonding strength demonstrated its ability to withstand most microfluidic applications, which is comparable to the plasma bonding method.

3.3. Computational fluid dynamics on the 3D vessel geometries

We used the software program Comsol Multiphysics version 5.3a with a laminar flow module to simulate the wall shear rate of the fluidic channel. In the laminar flow module, we assumed that there was incompressible flow, no turbulence, and a no-slip boundary condition. For this simulation, we applied a blood density of 1.080 g/mL and a dynamic viscosity of 3.5×10^{-3} Pa.s [39]. The mean flow of the inlet was set to 3 mL/hr. The outlet pressure was set to atmospheric pressure with no backflow. We simulated the four channels with elliptical cross-sections of 20 mm in length. In the device, there are four parallel channels to represent the four conditions, which are concentric and eccentric stenosis of 63 % and 84 % (Fig. 6). The actual dimensions of the channel were used to draw the 3D computer-aided design (CAD) model and they were imported to the Comsol software program to simulate the wall shear rate of the stenosis channels. The simulation results are shown in Fig. 7. According to our simulation, with the same mean flow rate of 3 mL/h, the 63 % and 84 % stenosis channels can generate peak wall shear rates of 1840 s^{-1} and 21,800 s^{-1}, respectively.

The major and minor axes of the elliptical cross-section are 500 μm and 400 μm, 200 μm and 150 μm, and 100 μm and 65 μm for the non-stenosis channel, 63 % stenosis channel, and 84 % stenosis channel, respectively. The stenosis was placed in the center of the channel for the 63 % and 84 % stenosis channels. The wall shear gradients with a 1 mm stenosis length were used, as shown in Fig. 7. The cross-section of the channel consists of an elliptical geometry; hence, we considered the

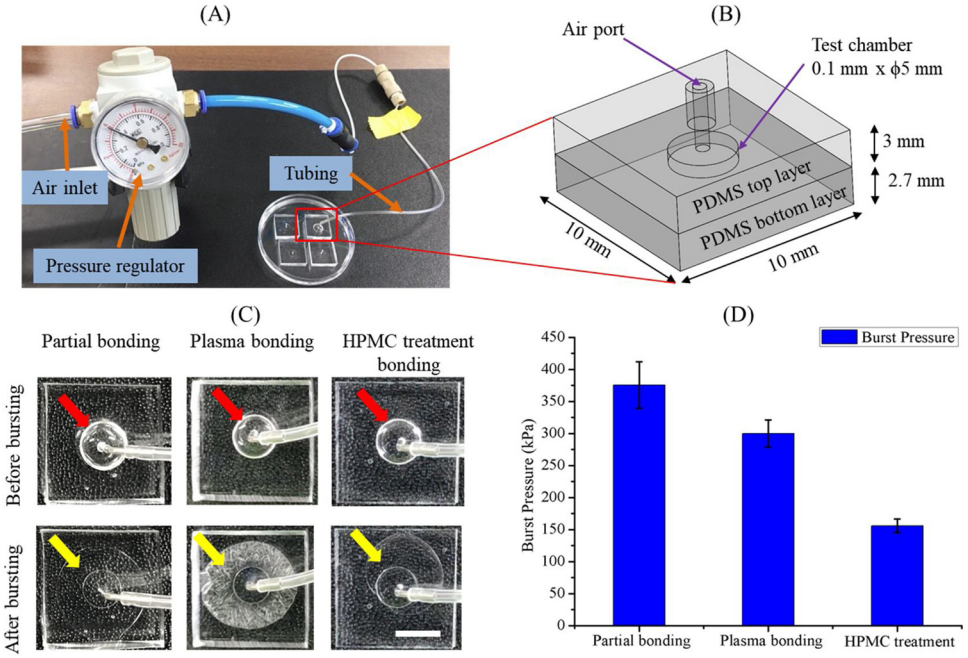

Fig. 5. Bonding strength testing with different bonding techniques. (A) Burst testing setup with air pressure regulator connected to air source at the inlet and testing device at the outlet (B) Zoom in the testing device with the top PDMS layer was connected to air source through inlet air-port. (C) The bright field images of the burst testing before and after bursting. Red arrows indicate the testing reservoir deformation due to high pressure before bonding busted. Yellow arrows indicate the bursted area after bonding failed. Scale bar, 5 mm. (D) The results of burst test with three bonding conditions of partially cured PDMS bonding, plasma bonding, and partially cured PDMS bonding with HPMC treatment. (For interpretation of the references to colour in the Figure, the reader is referred to the web version of this article).

wall shear rate for profile (a) and (b) for the concentric channels, and profiles (a), (b), and (c) for the eccentric channels. In general, the slope of the wall shear rate rapidly increased and decreased with vessel contraction and expansion. Depending on the channel profile, the peak of the shear rate was different for each profile. At 63 % stenosis, the maximum shear rate was placed at the center of the stenosis on profile (b) with 1840 s^{-1}, and 1930 s^{-1} for concentric and eccentric, respectively. At 84 % stenosis, the maximum shear rate was placed at the center of profile (b) with 21,800 s^{-1} and 21,593 s^{-1} for the concentric and eccentric channels, respectively.

3.4. Thrombus growth under different channel geometry

To perfuse the whole blood, one end of the four channels was connected to the outlet; the other end was punched for the inlet of the blood flow (Fig. 6C). The cross-sectional diameter is gradually changed from a normal diameter to stenosis and then back to normal (Fig. 6A). The results of the stenosis channels are presented in Fig. 8 with a uniform channel cross-section. In order to investigate the effect of the stenosis lesion on the stability of the thrombus, we perfused the whole blood within 5 min for each channel. The stenosis length was 1 mm with the circular cross-section that is depicted in Fig. 8, where the geometry was constricted at the center of the stenosis length. Thrombus formation was initiated through adhesion, where the flowing platelets met a thrombogenic surface (e.g. collagen) and it began to adhere. Platelet-platelet interaction was dominant during thrombus development [40].

Fig. 8 displays the geometry of the stenosis channel for the different levels and shapes of the stenosis. The circular cross-section of the vessel defined the 3D stenosis geometry before stenosis, then it gradually reduced the diameter to the center of the stenosis with a smooth surface. These geometries typically were found in the clinical atherosclerosis

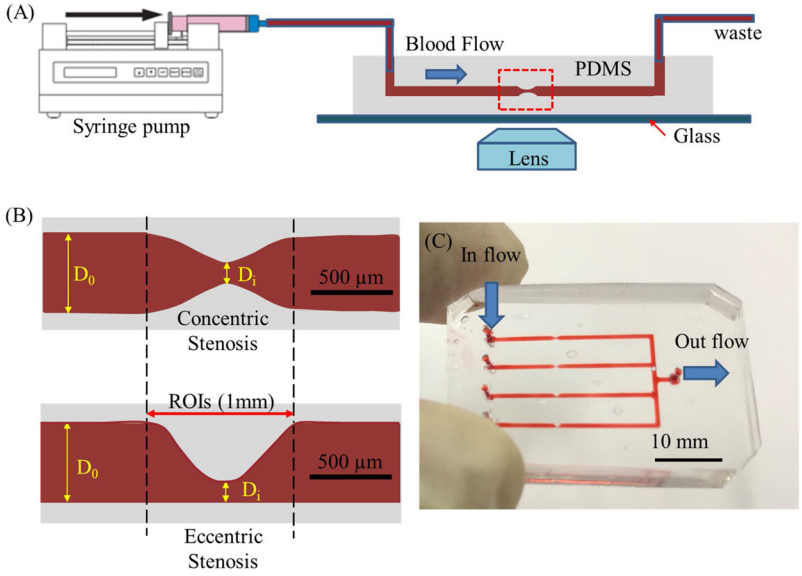

Fig. 6. (A) Schematic of the experimental setup with syringe pump used to perfuse the whole blood into the channel. The thrombus formation was observed under fluorescent microscopy. (B) Two types of lesion: concentric and eccentric (C) The PDMS device with four stenosis channels fills with food dye.

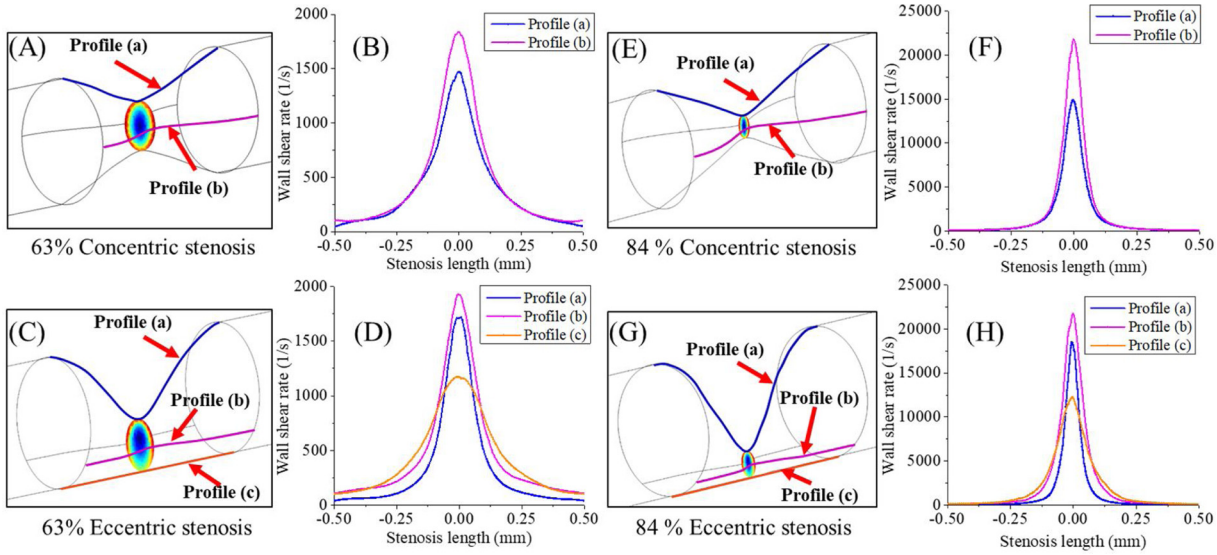

Fig. 7. Wall shear rate of different stenosis channel. (A) 63 % concentric stenosis. (B) Wall shear rate gradient along to profile (a) and profile (b) of 63 % concentric stenosis. (C) 63 % eccentric stenosis. (D) Wall shear rate gradient along to profile (a), profile (b), profile (c) of 63 % eccentric stenosis. (E) 84 % concentric stenosis. (F) Wall shear rate gradient along to profile (a) and profile (b). (G) 84 % eccentric stenosis. (H) Wall shear rate gradient along to profile (a), profile (b), profile (c).

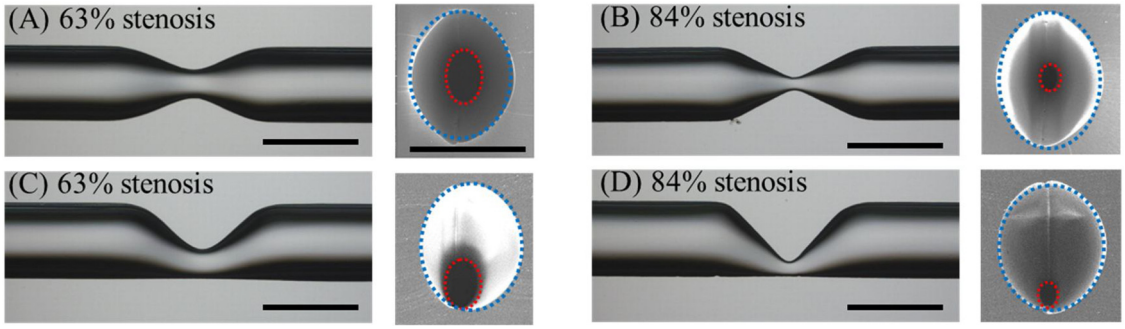

Fig. 8. Bright field image of the top view of stenosis channel and SEM images of the cross-section stenosis microchannel. (A) 63 % concentric stenosis, (B) 84 % concentric stenosis. (C) 63 % eccentric stenosis, (D) 84 % eccentric stenosis. The right hand side of each bright field image is an SEM image of the cross-sectional microchannel. The blue dash line shows the channel before stenosis, the red dash line shows the stenosis diameter. Scale bar, 500 μm. (For interpretation of the references to colour in the Figure, the reader is referred to the web version of this article).

blood vessel [10,39]. To our knowledge, this is the first study to investigate the association between the concentric and eccentric stenosis of the circular channel and the formation of thrombosis-on-a-chip. Whole blood perfusion through the 63 % stenosis and 84 % stenosis channels showed that thrombosis only occurred in the microfluidic channels for 84 % stenosis and there was no sign of thrombus formation for the 63 % stenosis channel at a shear rate level of 1840 s^{-1} after 5 min of perfusion (data not shown). In a living vessel, the high shear rate thrombosis takes place in pathological flow with a high stenosis percentage vessel such as an atherosclerotic vessel. Rupture of the atherosclerotic plaque will expose the thrombosis factors on the blood vessel wall, which can result in thrombosis formation and clotting. This event occurs in a very short time (less than 1 min) [15]. Therefore, the perfusion time of 5 min is appropriate for thrombosis formation. There are two different biological mechanisms which can lead to thrombus: (a) the coagulation cascade of protein activation and (b) cellular platelet aggregation thrombosis. Even though coagulation dominates thrombus formation at low shear rates (e.g. $< 50\ s^{-1}$), it can lead to red clots. By contrast, by having wall shear rates higher than 5000 s^{-1}, platelet accumulation dominates, which can lead to white clots that occur during pathological flow in arteries [41]. Here, we propose to mimic high shear rate thrombosis for a stenosis blood vessel to activate platelet accumulation. Therefore, platelet accumulation can be considered for thrombosis formation. On the other hand, in the case of 84 % stenosis, accumulation of the thrombus rapidly formed downstream of the stenosis due to the high shear rate in the stenosis ($> 10{,}000\ s^{-1}$); vWF likely played a crucial role in recruiting the platelets to the thrombus. Thrombus formation was initiated through adhesion, where the flowing platelets met a thrombogenic surface (e.g. collagen) and it began to adhere. Platelet-platelet interaction was dominant during thrombus development [40]. The intensity of the thrombus indicates the platelet activation for aggregation. Stick and slip mechanics were observed during the growth of the thrombus with multiple peaks in intensity. The average intensity in the case of the concentric was much higher than eccentric thrombosis (Fig. 9).

Interestingly, despite having the same stenosis percentage, the platelet formation for concentric and eccentric geometries was different where the concentric geometry can create symmetric platelet accumulation (shown in Fig. 9A, B). The concentric geometry gradually changed the diameter and had more symmetrical flow, thereby leading to more symmetric thrombus growth. Fig. 9C shows the steady increase in the thrombus until embolization occurred and prompted the sharp drop in the intensity. On the other hand, the eccentric geometry allowed for thrombus growth on one side of the channel where there was a higher deceleration flow (shown in Fig. 9D). Eccentric stenosis with the asymmetric accumulation changed the flow directions downstream of the stenosis, which makes thrombus formation unstable. The phenomenon of the shear rate gradients that influences thrombus

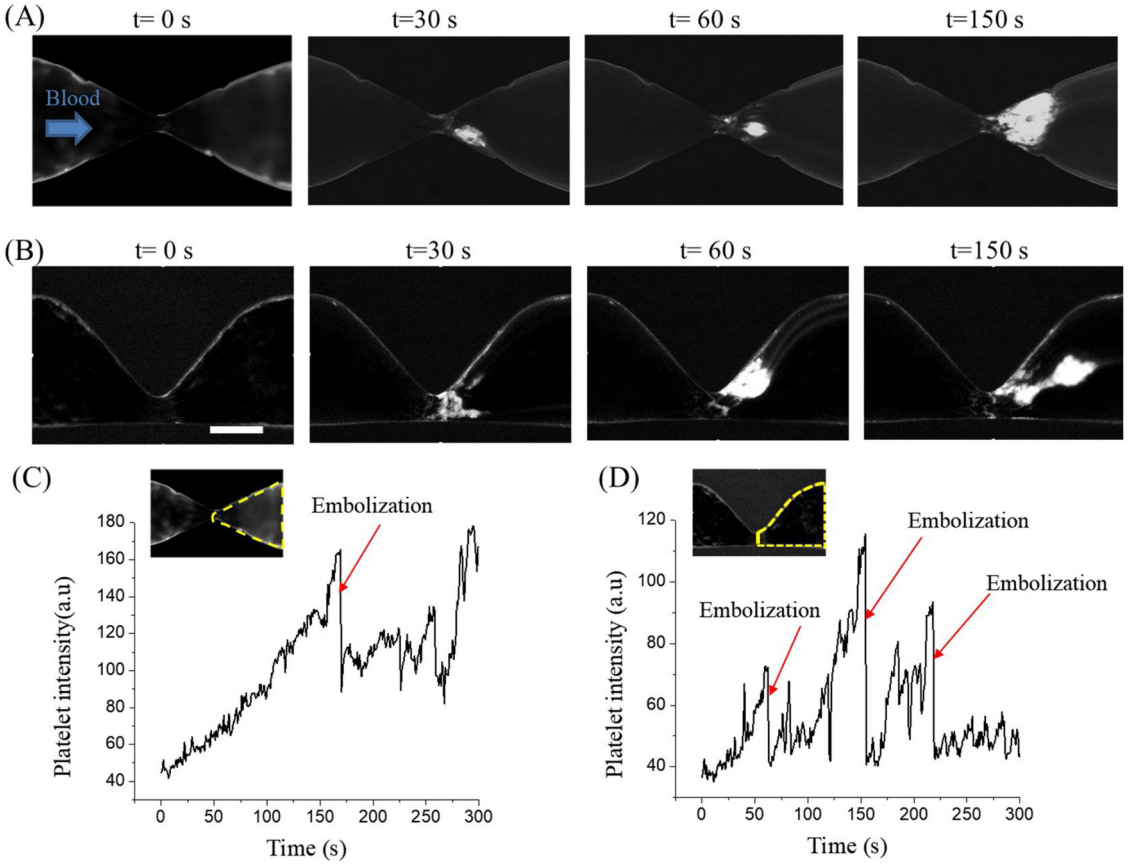

Fig. 9. The platelet accumulation at the downstream of stenosis channel. (A), (B) Fluorescent images of platelet accumulation of 84 % concentric stenosis and eccentric stenosis with 3 mL/hr flow rate of the whole blood, respectively. The white area shown the thrombus growth at the post stenosis vessel (C), (D) The average fluorescent intensity of platelet accumulation. The sharp drop of the intensity indicate the embolization of the thrombus. Scale bar, 200 μm.

formation has recently been described in rectangular stenosis channels [15,10]. Our data of circular stenosis geometry significantly enhances the previous findings since it demonstrates the importance of vWF acting as a regulator of the platelet aggregation at post stenotic sites with a rapidly decreasing wall shear rate.

We compared the wall shear rate and the platelet aggregation time with the in vivo model where a high shear rate at the stenosis vessel promotes platelet accumulation. Nesbitt et al. [15] employed intravital imaging to visualize the platelet aggregation process in the arterioles of mice. Localized stenosis markedly accelerated the rate and the extent of the platelet aggregation at 16.39 s when stenosis was greater than 90 %. The flow accelerates into the stenosis throat and reaches a maximum shear of > 20,000 s^{-1} at the apex. Our stenosis channels are able to reach a similar level of shear rate (21,800 s^{-1} at 84 % stenosis channel) as presented during in vivo thrombosis. In addition, the proposed stenosis channels also show rapid platelet accumulation (Fig. 9A) for concentric and eccentric stenosis. Indeed, a direct comparison with the in vivo conditions is difficult to obtain due to the discrimination on the experiment conditions. However, with a microfluidic channel, a high shear microgradient is easy to obtain by using a stenosis channel. Moreover, the channel geometry can be engineered to closely mimic the in vivo blood vessel such as the circular geometry and the eccentricity of the stenosis. In addition, in vitro flow with the microfluidics channel takes advantage in matching the wall shear rate with the in vivo phenomena for rapid platelet accumulation while using a small volume of blood.

The embolization event is identified by the sharp drop and then it gradually increases the areal fluorescent intensity of the platelet aggregation in Fig. 9C and D. The red arrows in Fig. 9C and D point to the event of the embolization with a sharp drop and followed it steadily with an accumulation of platelets. The details of the embolization event are presented in Fig. 10; the left images indicate the thrombus before dislodging. Embolization happens after 179 s for the concentric stenosis channels, whereas eccentric stenosis embolization takes place at 62 s, 154 s, and 217 s.

The difference in the shear rate gradient along the stenosis region influences the thrombus formation and the fractional flow reverse value [39]. Thrombus formation may be accelerated in the regions of the platelets during recirculation, high shearing, and increased turbulence [42]. This can explain the faster embolus formation in comparison to concentric stenosis. The results indicate the important role of the plaque shape (concentric or eccentric), which is typically not considered in a standard diagnosis, in addition to stenosis severity.

We assume that the value of the platelet intensity is directly proportional to the size of the thrombus. A higher intensity of the platelet accumulation results in a bigger thrombus. Therefore, the stability of the thrombus presents a steadily increasing thrombus size and less thrombus dislodging. We evaluated the stability of the thrombus based on the number of thrombus embolization events, which is one time for concentric stenosis and three times for eccentric stenosis during 5 min of perfusion (Fig. 10). The amplitude of the dropped intensity can be correlated to the embolus size. The dropped intensity of the concentric stenosis is 73.4 a.u. For eccentric stenosis, the dropped intensities are 32.3 a.u, 72.8 a.u, and 45.6 a.u for the first, second, and third embolization event, respectively. From these preliminary results, we can conclude that the thrombus stability and the embolus size are directly correlated with the stenosis geometry. Owing to the longer compaction time of the thrombus, an embolism is larger for the concentric stenosis than for the eccentric stenosis (Movie S1, S2).

Moreover, the results indicate that the thrombus building up in the

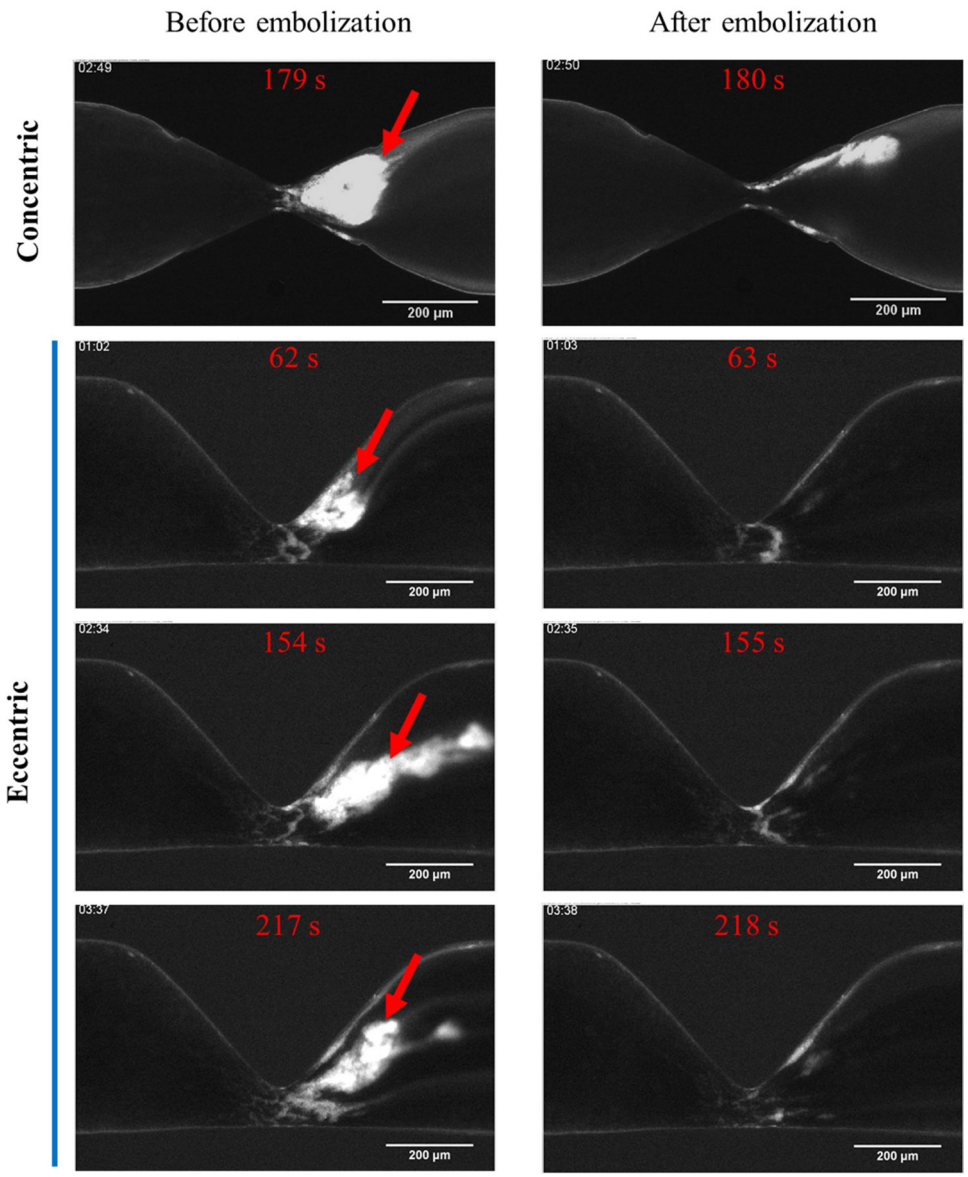

Fig. 10. The embolization event of concentric and eccentric stenosis channel. Left column shown the thrombus before embolization at different time point. Red arrows point the thrombus position. Right column indicates the stenosis channel after thrombus dislodged. (For interpretation of the references to colour in the Figure, the reader is referred to the web version of this article).

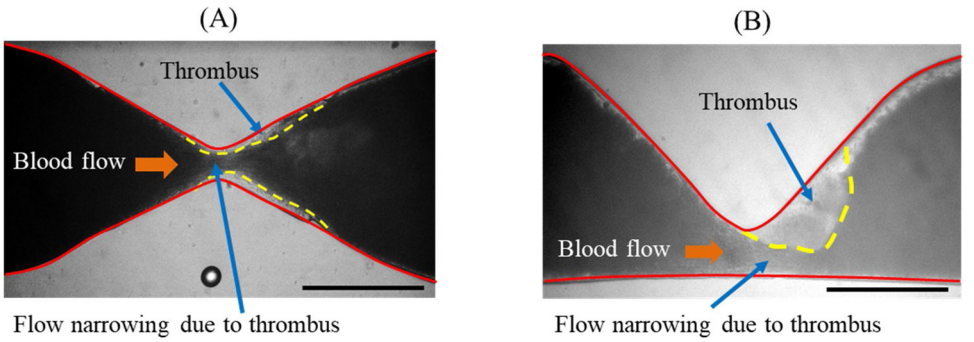

Fig. 11. The thrombus accumulation at the stenosis channel caused of the vessel narrowing. (A) Concentric stenosis. (B) Eccentric stenosis. Red lines show the boundary of the PDMS vessel, yellow dash lines indicate the thrombus accumulation on the vessel surface that narrowing the blood flow through stenosis channel. Scale bar, 200 μm. (For interpretation of the references to colour in the Figure, the reader is referred to the web version of this article).

stenosis channel will significantly reduce the vessel diameter. The narrowing is due to permanent platelet adhesion and the fibrin accumulation downstream of the stenosis after the blood perfusion as shown in Fig. 11 and Movies S3 and S4. The narrowing of the vessel lumen occurs on both sides for a concentric case (Fig. 11A) and on one side for an eccentric case (Fig. 11B).

4. Conclusions

In summary, we present an inexpensive and simple method that can

fabricate multiple diameters of the circular microfluidic channels from 100 µm to 500 µm. Since the internal pressure of the channel is well controlled, the repeatability of the fabricated channels is improved over the previous methods. Moreover, in the same mold design, we obtained a variety of different cross-sections of the channels by combining different fabrication conditions for the first and second halves of the channels. The device itself enables plasma-free activation and auto-aligned bonding with a bonding strength of 375 kPa, which is suitable for most microfluidics applications. By using a collagen-coated channel of 63 % and 84 % stenosis geometry, we successfully recapitulated the clinically derived physiological wall shear rate (1840 s^{-1}) and pathological flow conditions at a high wall shear rate (21,800 s^{-1}). For the first time, the 3D morphology of the stenosis vessel was considered to investigate the thrombosis formation and the stability. We found that the thrombosis growth for the concentric stenosis is more stable than eccentric stenosis and it also creates a bigger embolus downstream of the stenosis. Finally, this fabrication method is a highly efficient, low-cost solution to design highly customized circular cross-section channels to evaluate the clotting events in the pathological blood vessels. It is a useful testing device for antiplatelet and anticoagulant therapeutics.

In future studies, this device can be used as a basic research tool for investigating artery morphology that affects the diameter stenosis, stenosis length, and the eccentricity. Currently, we coat the channels with a thrombogenic factor to initially activate the platelet adhesion; however, future studies should utilize an endothelial cell coating on the channel to improve the accuracy of mimicking a real blood vessel.

CRediT authorship contribution statement

Thanh Qua Nguyen: Conceptualization, Methodology, Data curation, Writing - original draft. **Woo-Tae Park:** Supervision, Writing - review & editing.

Declaration of Competing Interest

The authors declare that they have no known competing financial interests or personal relationships that could have appeared to influence the work reported in this paper.

Acknowledgements

This work was supported by the Mid-Career Researcher Program under the National Research Foundation of Korea (NRF-2017R1A2B4011556).

Appendix A. Supplementary data

Supplementary material related to this article can be found, in the online version, at doi:https://doi.org/10.1016/j.snb.2020.128590.

References

[1] A. Bernardo, et al., Von Willebrand factor present in fibrillar collagen enhances platelet adhesion to collagen and collagen-induced platelet aggregation, J. Thromb. Haemost. 2 (4) (2004) 660–669, https://doi.org/10.1111/j.1538-7836.2004.00661.x.

[2] T.V. Colace, S.L. Diamond, Direct observation of von Willebrand factor elongation and fiber formation on collagen during acute whole blood exposure to pathological flow, Arterioscler. Thromb. Vasc. Biol. 33 (1) (2013) 105–113, https://doi.org/10.1161/ATVBAHA.112.300522.

[3] D.A. Vorchheimer, R. Becker, Platelets in atherothrombosis, Mayo Clin. Proc. 81 (1) (2006) 59–68, https://doi.org/10.4065/81.1.59.

[4] P. Jagadeeswaran, B.C. Cooley, P.L. Gross, N. Mackman, Animal models of thrombosis from zebrafish to nonhuman Primates: use in the elucidation of new pathologic pathways and the development of antithrombotic drugs, Circ. Res. 118 (9) (2016) 1363–1379, https://doi.org/10.1161/CIRCRESAHA.115.306823.

[5] Y. Xia, G.M. Whitesides, Soft lithography, Annu. Rev. Mater. Sci. 28 (1) (1998) 153–184, https://doi.org/10.1146/annurev.matsci.28.1.153.

[6] R. Van Kruchten, J.M.E.M. Cosemans, J.W.M. Heemskerk, Measurement of whole blood thrombus formation using parallel-plate flow chambers a practical guide, Platelets 23 (3) (2012) 229–242, https://doi.org/10.3109/09537104.2011.630848.

[7] N.K.R. Pandian, R.G. Mannino, W.A. Lam, A. Jain, Thrombosis-on-a-chip: prospective impact of microphysiological models of vascular thrombosis, Curr. Opin. Biomed. Eng. 5 (November 2017) (2017) 29–34, https://doi.org/10.1016/j.cobme.2017.12.001.

[8] K. Konstantopoulos, S. Kukreti, L.V. McIntire, Biomechanics of cell interactions in shear fields, Adv. Drug Deliv. Rev. 33 (1–2) (1998) 141–164, https://doi.org/10.1016/S0169-409X(98)00024-6.

[9] M. Li, D.N. Ku, C.R. Forest, Microfluidic system for simultaneous optical measurement of platelet aggregation at multiple shear rates in whole blood, Lab Chip 12 (7) (2012) 1355–1362, https://doi.org/10.1039/c2lc21145a.

[10] E. Westein, A.D. van der Meer, M.J.E. Kuijpers, J.-P. Frimat, A. van den Berg, J.W.M. Heemskerk, Atherosclerotic geometries exacerbate pathological thrombus formation poststenosis in a von Willebrand factor-dependent manner, Proc. Natl. Acad. Sci. 110 (4) (2013) 1357–1362, https://doi.org/10.1073/pnas.1209905110.

[11] P.F. Costa, et al., Mimicking arterial thrombosis in a 3D-printed microfluidic: in vitro vascular model based on computed tomography angiography data, Lab Chip 17 (16) (2017) 2785–2792, https://doi.org/10.1039/c7lc00202e.

[12] B. Sebastian, P.S. Dittrich, Microfluidics to mimic blood flow in health and disease, Annu. Rev. Fluid Mech. 50 (1) (2017) 483–504, https://doi.org/10.1146/annurev-fluid-010816-060246.

[13] M. Li, N.A. Hotaling, D.N. Ku, C.R. Forest, Microfluidic thrombosis under multiple shear rates and antiplatelet therapy doses, PLoS One 9 (1) (2014), https://doi.org/10.1371/journal.pone.0082493.

[14] B.A. Herbig, X. Yu, S.L. Diamond, Using microfluidic devices to study thrombosis in pathological blood flows, Biomicrofluidics 12 (4) (2018), https://doi.org/10.1063/1.5021769.

[15] W.S. Nesbitt, et al., A shear gradient-dependent platelet aggregation mechanism drives thrombus formation, Nat. Med. 15 (6) (2009) 665–673, https://doi.org/10.1038/nm.1955.

[16] A. Jain, A. Graveline, A. Waterhouse, A. Vernet, R. Flaumenhaft, D.E. Ingber, A shear gradient-activated microfluidic device for automated monitoring of whole blood haemostasis and platelet function, Nat. Commun. 7 (2016) 1–10, https://doi.org/10.1038/ncomms10176.

[17] S.M. Hastings, M.T. Griffin, D.N. Ku, Hemodynamic studies of platelet thrombosis using microfluidics, Platelets 28 (5) (2017) 427–433, https://doi.org/10.1080/09537104.2017.1316483.

[18] N.A. Mortensen, F. Okkels, H. Bruus, Reexamination of Hagen-Poiseuille flow: Shape dependence of the hydraulic resistance in microchannels, Phys. Rev. E - Stat. Nonlinear, Soft Matter Phys. 71 (5) (2005) 1–4, https://doi.org/10.1103/PhysRevE.71.057301.

[19] M. Lui, et al., Novel stenotic microchannels to study thrombus formation in shear gradients: Influence of shear forces and human platelet-related factors, Int. J. Mol. Sci. 20 (12) (2019) 1–10, https://doi.org/10.3390/ijms20122967.

[20] L.D.C. Casa, D.N. Ku, Geometric design of microfluidic chambers: platelet adhesion versus accumulation, Biomed. Microdevices 16 (1) (2014) 115–126, https://doi.org/10.1007/s10544-013-9811-7.

[21] T. Nguyen, S. Lee, W. Park, Novel circular microchannels fabrication method for artery thrombosis investigation, IEEE Micro Electro Mechanical Systems (January) (2018) 352–354.

[22] Y. Li, C. Pan, Y. Li, E. Kumacheva, A. Ramachandran, An exploration of the reflow technique for the fabrication of an in vitro microvascular system to study occlusive clots, Biomed. Microdevices 19 (4) (2017) 1–16, https://doi.org/10.1007/s10544-017-0213-0.

[23] M.E. Wilson, et al., Fabrication of circular microfluidic channels by combining mechanical micromilling and soft lithography, Lab Chip 11 (8) (2011) 1550–1555, https://doi.org/10.1039/c0lc00561d.

[24] R. He, D. Yunus, C. Uhl, W. Shi, S. Sohrabi, Y. Liu, Fabrication of circular microfluidic channels through grayscale dual-projection lithography, Microfluid. Nanofluidics 21 (1) (2017) 1–10, https://doi.org/10.1007/s10404-017-1851-5.

[25] J.S. Choi, Y. Piao, T.S. Seo, Fabrication of various cross-sectional shaped polymer microchannels by a simple PDMS mold based stamping method, Biochip J. 6 (3) (2012) 240–246, https://doi.org/10.1007/s13206-012-6306-1.

[26] J.M. Huffman, J. Shao, C.H. Hsu, A. Folch, Elastomeric molds with tunable microtopography, Adv. Mater. 16 (23–24) (2004) 2201–2206, https://doi.org/10.1002/adma.200400441.

[27] J. Xing, W. Rong, D. Sun, L. Wang, L. Sun, Rapid fabrication of rounded microchannels via extrusion printing of molds using a thixotropic ink, Sens. Actuators B Chem. 248 (March) (2017) 613–621, https://doi.org/10.1016/j.snb.2017.03.111.

[28] G. Pitingolo, R. Vecchione, A.P. Falanga, D. Guarnieri, P.A. Netti, Fabrication of a modular hybrid chip to mimic endothelial-lined microvessels in flow conditions, J. Micromech. Microeng. 27 (3) (2017), https://doi.org/10.1088/1361-6439/aa5a79.

[29] P.R. Hunziker, M.P. Wolf, X. Wang, B. Zhang, S. Marsch, G.B. Salieb-Beugelaar, Construction of programmable interconnected 3D microfluidic networks, J. Micromech. Microeng. 25 (2) (2015), https://doi.org/10.1088/0960-1317/25/2/025018.

[30] R. Sfriso, et al., 3D artificial round section micro-vessels to investigate endothelial cells under physiological flow conditions, Sci. Rep. 8 (1) (2018) 1–13, https://doi.org/10.1038/s41598-018-24273-7.

[31] S. Oh, S. Han, Y. Hwang, H. Yi, K. Kang, Fabrication of truly 3D microfluidic channel using 3D-printed soluble mold, Biomicrofluidics 12 (1) (2018) 014105, https://doi.org/10.1063/1.5012548.

[32] Y. Zheng, et al., In vitro microvessels for the study of angiogenesis and thrombosis, Proc. Natl. Acad. Sci. 109 (24) (2012) 9342–9347, https://doi.org/10.1073/pnas.1201240109.

[33] T.-Q. Nguyen, W.-T. Park, Rapid, low cost fabrication of circular cross-section microchannels by thermal air molding, Proceedings of the IEEE International Conference on Micro Electro Mechanical Systems (MEMS), vol. 2015-Febru, February, 2015, https://doi.org/10.1109/MEMSYS.2015.7050960.
[34] T.Q. Nguyen, W.T. Park, Rapid, low-cost fabrication of circular microchannels by air expansion into partially cured polymer, Sensors Actuators B Chem. 235 (2016) 302–308, https://doi.org/10.1016/j.snb.2016.05.008.
[35] L. Yang, X. Hao, C. Wang, B. Zhang, W. Wang, Rapid and low cost replication of complex microfluidic structures with PDMS double casting technology, Microsyst. Technol. 20 (10–11) (2014) 1933–1940, https://doi.org/10.1007/s00542-013-2004-8.
[36] E.J. Wong, Modeling and Control of Rapid Cure in Polydimethylsiloxane (PDMS) for Microfluidic Device Applications in Partial Fulfillment of the Requirements for the Degree of Doctor of Philosophy in Mechanical Engineering, (2010).
[37] I.P. Pinar, J.F. Arthur, R.K. Andrews, E.E. Gardiner, K. Ryan, J. Carberry, Methods to determine the lagrangian shear experienced by platelets during thrombus growth, PLoS One 10 (12) (2015) 1–14, https://doi.org/10.1371/journal.pone.0144860.
[38] M.A. Eddings, M.A. Johnson, B.K. Gale, Determining the optimal PDMS-PDMS bonding technique for microfluidic devices, J. Micromech. Microeng. 18 (6) (2008), https://doi.org/10.1088/0960-1317/18/6/067001.
[39] D.-Y. Kang, et al., Impact of coronary lesion geometry on fractional flow reserve, Circ. Cardiovasc. Imaging 11 (6) (2018), https://doi.org/10.1161/circimaging.117.007087.
[40] S. Kulkarni, et al., A revised model of platelet aggregation, J. Clin. Invest. 105 (6) (2000) 783–791, https://doi.org/10.1172/JCI7569.
[41] L.D.C. Casa, D.H. Deaton, D.N. Ku, Role of high shear rate in thrombosis, J. Vasc. Surg. 61 (4) (2015) 1068–1080, https://doi.org/10.1016/j.jvs.2014.12.050.
[42] T.L. Poepping, R.N. Rankin, D.W. Holdsworth, Flow patterns in carotid bifurcation models using pulsed doppler ultrasound: Effect of concentric vs. eccentric stenosis on turbulence and recirculation, Ultrasound Med. Biol. 36 (7) (2010) 1125–1134, https://doi.org/10.1016/j.ultrasmedbio.2010.02.005.

Thanh-Qua Nguyen received his M.Sc. in Seoul National University (Korea) in 2014 from the Multiscale Biomedical Engineering laboratory. He received a Ph.D. degree at Convergence Institute of Biomedical and Biomaterial Engineering at Seoul National University of Science and Technology in 2019. His current research interests include the development of rapid and low-cost fabrication technology for microfluidic devices and organ-on-a chip technology.

Woo-Tae Park received the B.S. degree in mechanical design from SungkyunkwanUniversity, Korea, in 2000, the M.S. and Ph.D. degrees in mechanical engineering from Stanford University in 2002 and 2006 respectively. For his Ph.D., he worked on wafer scale encapsulated MEMS devices for biomedical applications. After graduation, he worked at Intel Corporation, Freescale Semiconductor, and IME Singapore, leading several projects on MEMS development. He has authored more than 80 journals and refereed conference papers and has 20 issued and pending patents. He is currently an associate professor at Seoul National University of Science and Technology, conducting research on sensors, medical devices, and microelectronics packaging.